Journal of Sound and Vibration (1999) **228**(5), 1125–1144
Article No. jsvi.1999.2473, available online at http://www.idealibrary.com on IDEAL®

BIFURCATION AND AMPLITUDE MODULATED MOTIONS IN A PARAMETRICALLY EXCITED TWO-DEGREE-OF-FREEDOM NON-LINEAR SYSTEM

J.-C. JI AND L. YU

Theory of Lubrication and Bearing Institute, Xi'an Jiaotong University, Xi'an, 710049, *People's Republic of China*

AND

Y.-S. CHEN

Department of Mechanics, Tianjin University, Tianjin, 300072, *People's Republic of China*

(*Received* 4 *January* 1999, *and in final form* 23 *June* 1999)

The non-linear response of a T-shaped beam–mass structure is investigated theoretically and experimentally for the case of one-to-two internal resonance and principal parametric resonance of the lower mode. The method of multiple scales is used to determine four first order amplitude- and phase-modulation equations. The non-trivial steady state solutions are obtained from trivial solutions through pitchfork bifurcation. The Melnikov's method is used to predict the critical parameter at which the dynamical system possesses a Smale horseshoe type of chaos. To verify the analytical results, experiments were performed on the T-shaped beam–mass structure. The periodically amplitude-modulated motions and chaotically amplitude-modulated motions were observed during experiments. The results of the experiment showed good qualitative agreement with the theoretical predictions.

1. INTRODUCTION

Many mechanical structures can be modelled as a two-degree-of-freedom (d.o.f.) non-linear system subject to parametric excitation. For systems with quadratic non-linearities, if the natural frequencies are of 1 : 2 internal resonance, energy exchange takes place between two modes, and complicated motions can occur. Nayfeh [1, 2] studied the Hopf bifurcation and routes to chaos in the presence of a two-to-one internal resonance of a parametrically excited two-d.o.f. system with quadratic non-linearities. Feng and Sethna [3] investigated global bifurcation and chaos in a parametrically forced system with one–one resonance. Feng and Wiggins [4] presented the existence of chaos in a class of two-d.o.f., damped, strongly parametrically forced mechanical systems with broken O(2) symmetry. Banerjee and Bajaj [5] analyzed amplitude-modulated chaos in two-d.o.f. systems with quadratic non-linearities under external or parametric excitation.

0022-460X/99/501125 + 20 $30.00/0

Although extensive local and global analyses of two-d.o.f. systems with weak quadratic non-linearities under weak external or parametric excitations have been carried out, there has been little research on their experimental investigation. Balachandran and Nayfeh [6] employed an L-shaped beam–mass structure to conduct experiments, and successfully observed Hopf bifurcation and chaos in a two-d.o.f. with quadratic non-linearities under external excitation.

The purpose of this study is to theoretically and experimentally investigate the non-linear response of a parametrically excited two-d.o.f. non-linear system with quadratic non-linearities under principal parametric resonance to the lower mode. The method of multiple scales is used to derive four first-order ordinary differential equations for the modulation of the amplitudes and phases of two modes, which control the essential dynamics of the original system for sufficiently small motions near resonance. As is well known, fixed points of the averaged equations exhibit periodic solutions of the original system, periodic solutions of the averaged equations imply periodically amplitude-modulated motions of the original system, and chaotic solutions of the averaged equations indicate chaotically amplitude-modulated response for the original system. The Melnikov's method is used to predict the global bifurcation and chaos in the averaged system. Experiments were performed under principal parametric resonance of the lower mode. Periodic motions, periodically amplitude-modulated motions and chaotically amplitude-modulated motions were observed.

2. ANALYSIS

2.1. EQUATIONS OF MOTION

The model under consideration is shown in Figure 1, which is a T-shaped beam–mass structure. It consists of two light-weight beams and two concentrated masses. The response of the structure can be modelled by a two-mode approximation. If u_1 and u_2 are the generalized co-ordinates of these two modes, the resulting dimensionless equations of motion are derived by using Hamilton's principal and Galerkin's method as a two-d.o.f. non-linear system subject to

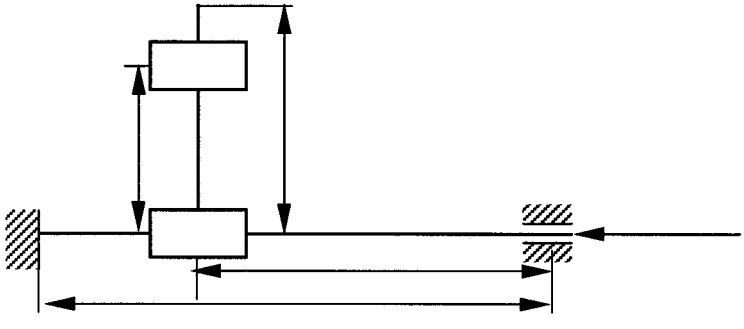

Figure 1. The two-d.o.f. mechanical structure. Horizontal beam: 1·15 mm × 31·75 mm × 416·5 mm, $\rho_1 = 0{\cdot}24258$ g/mm, $m_1 = 166{\cdot}7$ g; vertical beam: 1·08 mm × 26·35 mm × 200·5 mm, $\rho_2 = 0{\cdot}1585$ g/mm, $m_2 = 51{\cdot}35$ g.

parametric excitation [7]

$$\begin{Bmatrix} \ddot{u}_1 \\ \ddot{u}_2 \end{Bmatrix} + 2\varepsilon \begin{bmatrix} \mu_1 & 0 \\ 0 & \mu_2 \end{bmatrix} \begin{Bmatrix} \dot{u}_1 \\ \dot{u}_2 \end{Bmatrix} + \begin{bmatrix} \omega_1^2 & 0 \\ 0 & \omega_2^2 \end{bmatrix} \begin{Bmatrix} u_1 \\ u_2 \end{Bmatrix} + \varepsilon \begin{bmatrix} M_{11} & M_{12} & M_{13} \\ M_{21} & M_{22} & M_{23} \end{bmatrix} \begin{Bmatrix} \dot{u}_1^2 \\ \dot{u}_1\dot{u}_2 \\ \dot{u}_2^2 \end{Bmatrix}$$

$$+ \varepsilon \begin{bmatrix} N_{11} & N_{12} & N_{13} & N_{14} \\ N_{21} & N_{22} & N_{23} & N_{24} \end{bmatrix} \begin{Bmatrix} u_1\ddot{u}_1 \\ u_1\ddot{u}_2 \\ u_2\ddot{u}_1 \\ u_2\ddot{u}_2 \end{Bmatrix} + 2\varepsilon \cos \Omega T \begin{bmatrix} f_{11} & f_{12} \\ f_{21} & f_{22} \end{bmatrix} \begin{Bmatrix} u_1 \\ u_2 \end{Bmatrix} = 0, \qquad (1)$$

where the highest order of terms retained are quadratic, ε is a small dimensionless parameter, μ_1 and μ_2 are the modal damping coefficients, and f_{mn}, Ω, ω_n, M_{mn} and N_{mn} are the constants. The parameters f_{mn} and Ω depend on the excitation, whereas the parameters ω_n, M_{mn} and N_{mn} depend on the values of the two masses and the dimensions and properties of the two beams.

2.2. PERTURBATION ANALYSIS

The method of multiple scales [8] is employed to obtain an approximate solution of equations (1) in the form

$$u_1 = u_{10}(T_0, T_1) + \varepsilon u_{11}(T_0, T_1) + \cdots,$$
$$u_2 = u_{20}(T_0, T_1) + \varepsilon u_{21}(T_0, T_1) + \cdots, \qquad (2)$$

where $T_n = \varepsilon^n t$. In terms of the T_n, the time derivatives become

$$\mathrm{d}/\mathrm{d}t = D_0 + \varepsilon D_1 + \cdots,$$
$$\mathrm{d}^2/\mathrm{d}t^2 = D_0^2 + 2\varepsilon D_0 D_1 + \cdots, \qquad (3)$$

where $D_n = \partial/\partial T_n$.
Substituting equations (2) and (3) into equations (1) and equating coefficients of like powers of ε to zero yields

Order ε^0:

$$D_0^2 u_{10} + \omega_1^2 u_{10} = 0,$$
$$D_0^2 u_{20} + \omega_2^2 u_{20} = 0. \qquad (4)$$

Order ε^1:

$$\begin{aligned} D_0^2 u_{11} + \omega_1^2 u_{11} = &-2D_0D_1u_{10} - 2\mu_1 D_0 u_{10} - [M_{11}(D_0u_{10})^2 + M_{12}(D_0u_{10})(D_0u_{20}) \\ &+ M_{13}(D_0u_{20})^2] - [N_{11}u_{10}D_0^2u_{10} + N_{12}u_{10}D_0^2u_{20} + N_{13}u_{20}D_0^2u_{10} \\ &+ N_{14}u_{20}D_0^2u_{20}] - 2(f_{11}u_{10} + f_{12}u_{20})\cos\Omega T_0, \\ D_0^2 u_{21} + \omega_2^2 u_{21} = &-2D_0D_1u_{20} - 2\mu_2 D_0 u_{20} - [M_{21}(D_0u_{10})^2 + M_{22}(D_0u_{10})(D_0u_{20}) \\ &+ M_{23}(D_0u_{20})^2] - [N_{21}u_{10}D_0^2u_{10} + N_{22}u_{10}D_0^2u_{20} + N_{23}u_{20}D_0^2u_{10} \\ &+ N_{24}u_{20}D_0^2u_{20}] - 2(f_{21}u_{10} + f_{22}u_{20})\cos\Omega T_0. \end{aligned} \qquad (5)$$

The solutions of equations (4) can be expressed in the complex forms

$$u_{10} = A_1(T_1)\exp(\mathrm{i}\omega_1 T_0) + \bar{A}_1(T_1)\exp(-\mathrm{i}\omega_1 T_0),$$
$$u_{20} = A_2(T_1)\exp(\mathrm{i}\omega_2 T_0) + \bar{A}_2(T_1)\exp(-\mathrm{i}\omega_2 T_0), \tag{6}$$

where A_n are undetermined functions of T_1 at this level of approximation, and $\bar{A}_n$ are the complex conjugate of A_n. They can be determined by imposing the solvability conditions at the next level of approximation. On substituting equations (6) into equations (5), the particular solutions of the resulting equations contain secular terms of the form $T_0\exp(\pm\mathrm{i}\omega_1 T_0)$ and $T_0\exp(\pm\mathrm{i}\omega_2 T_0)$ and small-divisor terms, depending on the resonant conditions. To the first order approximation, these resonant conditions are (a) internal resonance $\omega_2 \cong 2\omega_1$ or $\omega_1 \cong 2\omega_2$; (b) principal parametric resonance of the higher mode $\Omega \cong 2\omega_1$; (c) principal parametric resonance of the lower mode $\Omega \cong 2\omega_2$; and (d) combination parametric resonances of the additive and difference types $\Omega \cong \omega_2 \pm \omega_1$.

In this paper, the principal parametric resonance of the lower mode ($\Omega \cong 2\omega_2$) is to be treated, in the presence of one-to-two internal resonance ($\omega_1 \cong 2\omega_2$). To describe quantitatively the nearness of these resonances, we introduce the detuning parameters σ_1, σ_2 as follows:

$$\Omega = 2\omega_2 + \varepsilon\sigma_1, \qquad \omega_1 = 2\omega_2 + \varepsilon\sigma_2. \tag{7}$$

Substituting equations (6) and (7) into equations (5), and eliminating the terms that produce secular terms in u_{11} and u_{21} yields the solvability conditions

$$-2\mathrm{i}\omega_1(A_1' + \mu_1 A_1) + J_1 A_2^2\exp(-\mathrm{i}\sigma_2 T_1) = 0,$$
$$-2\mathrm{i}\omega_2(A_2' + \mu_2 A_2) + J_2 A_1\bar{A}_2\exp(-\mathrm{i}\sigma_2 T_1) - f_{22}\bar{A}_2\exp(\mathrm{i}\sigma_1 T_1) = 0, \tag{8}$$

where $J_1 = M_{13}\omega_2^2 + N_{14}\omega_2^2$, $J_2 = -M_{22}\omega_1\omega_2 + N_{22}\omega_2^2 + N_{23}\omega_1^2$, and the prime indicates the derivative with respect to T_1.

In order to solve equations (8), we introduce the polar forms

$$A_1 = \frac{\sqrt{2}a_1^{1/2}}{J_2^2}\exp\left(\mathrm{i}\frac{\varphi_1}{\omega_1}\right), \qquad A_2 = \frac{\sqrt{2}a_2^{1/2}}{J_1 J_2}\exp\left(\mathrm{i}\frac{\varphi_2}{\omega_2}\right), \tag{9}$$

where a_i, φ_i are real functions of time T_1. Substituting equations (9) into equations (8) and separating the real and imaginary parts of the resulting equations yields the following set of amplitude- and phase-modulation equations:

$$a_1' = -2\mu_1 a_1 - \frac{\sqrt{2}}{\Omega}a_1^{1/2}a_2\sin(\theta_1 - 2\theta_2),$$

$$a_1\theta_1' = (\sigma_2 - \sigma_1)a_1 - \frac{\sqrt{2}}{2\Omega}a_1^{1/2}a_2\cos(\theta_1 - 2\theta_2),$$

$$a_2' = -2\mu_2 a_2 + \frac{2\sqrt{2}}{\Omega}a_1^{1/2}a_2\sin(\theta_1 - 2\theta_2) + \frac{2f_{22}}{\Omega}a_2\sin(2\theta_2),$$

$$a_2\theta_2' = -\frac{\sigma_1}{2}a_2 - \frac{\sqrt{2}}{\Omega}a_1^{1/2}a_2\cos(\theta_1 - 2\theta_2) + \frac{f_{22}}{\Omega}a_2\cos(2\theta_2), \tag{10}$$

where $\theta_1 = (\varphi_1/\omega_1) + (\sigma_2 - \sigma_1)T_1$, $\theta_2 = (\varphi_2/\omega_2) - (\sigma_1/2)T_1$, $i = 1, 2$. In the investigation of the stability of the trivial solutions, it is important to transform equations (10) into the Cartesian form in order to avoid dividing by a_1 and a_2. By using the change of variables

$$u_i = \sqrt{2a_i}\cos\theta_i, \quad v_i = -\sqrt{2a_i}\sin\theta_i, \quad i = 1, 2 \tag{11}$$

in equations (10), one can obtain

$$\begin{aligned}
u_1' &= -c_1u_1 + (\sigma_2 - \sigma_1)v_1 - \frac{1}{\Omega}u_2v_2,\\
v_1' &= -c_1v_1 - (\sigma_2 - \sigma_1)u_1 + \frac{1}{2\Omega}(u_2^2 - v_2^2),\\
u_2' &= -c_2u_2 - \frac{\sigma_1}{2}v_2 + \frac{1}{\Omega}(u_1v_2 - v_1u_2) - \frac{f_{22}}{\Omega}v_2,\\
v_2' &= -c_2v_2 + \frac{\sigma_1}{2}u_2 + \frac{1}{\Omega}(u_1u_2 + v_1v_2) - \frac{f_{22}}{\Omega}u_2,
\end{aligned} \tag{12}$$

Here, we have let $c_i = \mu_i$ for the sake of clearness. The Hamiltonian function corresponding to the averaged equations (10) without damping can be written as

$$H = (\sigma_2 - \sigma_1)a_1 - \frac{\sqrt{2}}{\Omega}a_1^{1/2}a_2\cos(\theta_1 - 2\theta_2) - \frac{\sigma_1}{2}a_2 + \frac{f_{22}}{\Omega}a_2\cos(2\theta_2), \tag{13}$$

where $a_i' = -\partial H/\partial\theta_i$, $\theta_i' = \partial H/\partial a_i$, $i = 1, 2$.

2.3. STEADY STATE SOLUTIONS AND BIFURCATION ANALYSIS

The stability and bifurcation of the steady state solutions of equations (1) are studied in this section. Periodic solutions of equations (1) correspond to the fixed points of equations (10), which are obtained by setting $a_i' = 0$ and $\theta_i' = 0$, $i = 1, 2$. There are two possibilities: either trivial solutions

$$a_1 = a_2 = 0, \tag{14}$$

or non-trivial solutions

$$a_1 = \frac{1}{2\Omega^2[c_1^2 + (\sigma_2 - \sigma_1)^2]}a_2^2, \tag{15a}$$

$$a_2 = [\tfrac{1}{2}\sigma_1(\sigma_1 - \sigma_2) - c_1c_2]\Omega^2 \pm \Omega^2\sqrt{F}, \tag{15b}$$

$$\sin(\theta_1 - 2\theta_2) = -\frac{\sqrt{2}c_1\Omega a_1^{1/2}}{a_2}, \tag{15c}$$

$$\sin(2\theta_2) = \frac{\Omega}{f_{22}}\left(c_2 + 2c_1\frac{a_1}{a_2}\right), \tag{15d}$$

where $F = (f_{22}^2/\Omega^2)[c_1^2 + (\sigma_1 - \sigma_2)^2] - [c_2(\sigma_1 - \sigma_2) + \frac{1}{2}\sigma_1 c_1]^2$, and θ_1 and θ_2 can be obtained from equations (15c) and (15d).

Therefore, to the first approximation, the response is trivial or given by

$$u_1 = \frac{2\sqrt{2}}{J_2^2} a_1^{1/2} \cos(\Omega t + \theta_1) + \cdots,$$

$$u_2 = \frac{2\sqrt{2}}{J_1 J_2} a_1^{1/2} \cos(\tfrac{1}{2}\Omega t + \theta_2) + \cdots, \tag{16}$$

where a_1 and a_2 are defined in equations (15a) and (15b) and θ_1 and θ_2 can be obtained from equations (15c) and (15d).

Next, one can determine the conditions under which equation (15b) has real roots. Obviously, it is required that $F \geqslant 0$, that is

$$f_{22} \geqslant \frac{c_2(\sigma_1 - \sigma_2) + \frac{1}{2}c_1\sigma_1}{[c_1^2 + (\sigma_1 - \sigma_2)^2]^{1/2}} \Omega = f_{20}$$

for the existence of real solutions of a_2 in equation (15b). There are two different cases for the real solutions of a_2 depending on the sign of the quantity $[\frac{1}{2}\sigma_1(\sigma_1 - \sigma_2) - c_1 c_2]$.

Case I: $[\frac{1}{2}\sigma_1(\sigma_1 - \sigma_2) - c_1 c_2] > 0$.

(i) a_2 has one positive root, when $f_{22} > \Omega(c_2^2 + \frac{1}{4}\sigma_1^2)^{1/2}$, which is given in equation (15b) as a_2^+.

(ii) a_2 has two positive roots which are given in equation (15b) as $a_2^\pm$, when $f_{20} \leqslant f_{22} \leqslant \Omega(c_2^2 + \frac{1}{4}\sigma_1^2)^{1/2}$.

Case II: $[\frac{1}{2}\sigma_1(\sigma_1 - \sigma_2) - c_1 c_2] < 0$.

(i) a_2 has one trivial root, when $f_{22} < \Omega(c_2^2 + \frac{1}{4}\sigma_1^2)^{1/2}$.

(ii) a_2 has one positive root which is given in equation (15b) as a_2^+ when $f_{22} > \Omega(c_2^2 + \frac{1}{4}\sigma_1^2)^{1/2}$.

In order to study the stability of fixed points of the averaged system (10), we need to investigate the characteristic equation of the Jacobian matrix of the averaged equations (12). Firstly, the eigenvalues of the Jacobian matrix for the trivial solutions ($u_i = v_i = 0$) can be written as

$$\lambda_{1,2} = -c_1 \pm \mathrm{i}\sqrt{(\sigma_2 - \sigma_1)^2}, \quad \lambda_{3,4} = -c_2 \pm \left(\frac{f_{22}^2}{\Omega^2} - \frac{1}{4}\sigma_1^2\right)^{1/2}. \tag{17}$$

Since the damping coefficients c_1, c_2 are always positive, the trivial solutions are asymptotically stable when $f_{22} < \Omega(c_2^2 + \frac{1}{4}\sigma_1^2)^{1/2}$, and unstable when $f_{22} > \Omega(c_2^2 + \frac{1}{4}\sigma_1^2)^{1/2}$. A pitchfork bifurcation occurs at $f_{22} = \Omega(c_2^2 + \frac{1}{4}\sigma_1^2)^{1/2}$, where an eigenvalue changes its sign from negative to positive. Thus, the trivial solutions lose their stability through pitchfork bifurcation giving rise to the non-trivial solutions. Secondly, the characteristic equation of the Jacobian matrix of the averaged

equations (12) for the non-trivial solutions can be written as

$$\lambda^4 + r_3\lambda^3 + r_2\lambda^2 + r_1\lambda + r_0 = 0, \tag{18}$$

where

$$r_3 = 2(c_1 + c_2), \quad r_2 = (\sigma_2 - \sigma_1)^2 + \frac{4a_2}{\Omega^2} + 4c_1c_2 + c_1^2,$$

$$r_1 = 2c_1^2c_2 + 2c_2(\sigma_2 - \sigma_1)^2 + \frac{4(c_1 + c_2)}{\Omega^2}\, a_2,$$

$$r_0 = \frac{4a_2}{\Omega^2}\left[\frac{a_2}{\Omega^2} + c_1c_2 - \frac{1}{2}\,\sigma_1(\sigma_1 - \sigma_2)\right].$$

According to the Routh–Hurwitz criterion, the necessary and sufficient conditions for all the eigenvalues have negative real parts are

$$(r_3r_2 - r_1) > 0, \quad r_1(r_3r_2 - r_1) - r_3^2r_0 > 0, \quad r_0 > 0, \tag{19}$$

where $(r_3r_2 - r_1) = 8(c_1 + c_2)c_1c_2 + 2c_1^3 + 2c_1(\sigma_2 - \sigma_1)^2 + 4(c_1 + c_2)a_2/\Omega^2$. It is easy to see that the first condition of equation (19) is automatically satisfied for positive damping parameters. If $r_0 < 0$, the second condition of equation (19) is satisfied, and so equation (18) has real positive roots if and only if $r_0 < 0$, i.e., $[(a_2/\Omega^2) + c_1c_2 - \frac{1}{2}\sigma_1(\sigma_1 - \sigma_2)] < 0$, which, in conjunction with equation (15b), implies that the fixed point corresponding to positive sign in equation (15b) is stable and that corresponding to the negative is unstable. The violation of the second condition in equation (19) would imply the existence of a pair of complex conjugate eigenvalues having a positive real part. Hence, replacing the inequality by an equality yields the parameters corresponding to Hopf bifurcation.

2.4. GLOBAL BIFURCATION: THE MELNIKOV'S METHOD

In order to use the modified version of Melnikov's method as in Wiggins [9], it is required to transform the averaged equations (10) to his desired form. To achieve this, we introduce the following canonical transformations to equations (10):

$$q_1 = \theta_1 - 2\theta_2,\ q_2 = \theta_2,\ p_1 = a_1,\ p_2 = a_2 + 2a_1, \tag{20}$$

and rescale the state variables and system parameters by $p_1 \to p_1/\alpha$, $p_2 \to p_2/\alpha$, $f_{22}/\Omega = \varepsilon_1 f$, $2c_1 = \varepsilon_1\delta_1$, $2c_2 = \varepsilon_1\delta_2$, where $\alpha = 2/\Omega^2$, $0 < \varepsilon_1 \ll 1$. We have

$$\begin{aligned}
p_1' &= -(p_2 - 2p_1)p_1^{1/2}\sin q_1 - \varepsilon_1\delta_1 p_1,\\
q_1' &= \sigma_2 - \tfrac{1}{2}p_1^{-1/2}(p_2 - 6p_1)\cos q_1 - \varepsilon_1 2f\cos(2q_2),\\
p_2' &= \varepsilon_1[-\delta_1 p_1 - \delta_2(p_2 - 2p_1) + 2f(p_2 - 2p_1)\sin(2q_2)],\\
q_2' &= -\tfrac{1}{2}\sigma_1 - p_1^{1/2}\cos q_1 + \varepsilon_1 f\cos(2q_2).
\end{aligned} \tag{21}$$

In order to calculate the Melnikov integral, it is required that we understand the geometry of the corresponding unperturbed system. The equations of the corresponding unperturbed system can be derived from equations (21) by letting $\varepsilon_1 = 0$, which can be expressed as

$$\begin{aligned} p_1' &= -(p_2 - 2p_1)p_1^{1/2}\sin q_1, \\ q_1' &= \sigma_2 - \tfrac{1}{2}p_1^{-1/2}(p_2 - 6p_1)\cos q_1, \\ p_2' &= 0, \\ q_2' &= -\tfrac{1}{2}\sigma_1 - p_1^{1/2}\cos q_1. \end{aligned} \tag{22}$$

Clearly, $p_{20} = I$ is a constant solution by the third equation of equation (22). Since a_1 and a_2 are proportional to the square of the amplitudes of response [refer to equations (16)] and p_{20} is a combination of the actions a_1 and a_2 of the averaged equations by the definitions (20), in some sense I represents the total mechanical energy of the system. The first two equations of equation (22) are independent with q_2, so we only need to consider the geometric structure of the unperturbed p_1–q_1 phase space. The Hamiltonian function for the $p_1 - q_1$ component of equations (22) is given by

$$H(p_1, q_1; p_2) = \sigma_2 p_1 - (I - 2p_1)p_1^{1/2}\cos q_1. \tag{23}$$

By noting the periodicity of q_1 and the transformations (20), the variables p_1 and q_1 can be restricted to the range $0 \leqslant p_1 \leqslant \frac{1}{2}I$ and $0 \leqslant q_1 \leqslant 2\pi$. In subsequent sections, we describe the geometric structure of the unperturbed (p_1, q_1) phase space. The equilibrium points of the first two equations in equation (22) can be determined for two different cases depending on the quantity σ_2.

(a) $I > \sigma_2^2/2$.

- When $\sigma_2 > 0$, the equilibrium points are

$$\text{(I)}\ \ p_1 = \tfrac{1}{2}I,\ q_1 = \cos^{-1}\left[-\frac{\sigma_2}{\sqrt{2I}}\right] = q_1^*, \tag{24}$$

$$\text{(II)}\ \ p_1 = p_1^- = \frac{3I + \sigma_2^2 - \sqrt{\sigma_2^4 + 6I\sigma_2^2}}{18},\ q_1 = 0, \tag{25}$$

$$\text{(III)}\ \ p_1 = p_1^+ = \frac{3I + \sigma_2^2 + \sqrt{\sigma_2^4 + 6I\sigma_2^2}}{18},\ q_1 = \pi; \tag{26}$$

- When $\sigma_2 < 0$, the equilibrium points are

$$\text{(I)}\ \ p_1 = \tfrac{1}{2}I,\ q_1 = \cos^{-1}\left[-\frac{\sigma_2}{\sqrt{2I}}\right] = q_1^*, \tag{27}$$

$$\text{(II)}\ \ p_1 = p_1^+ = \frac{3I + \sigma_2^2 + \sqrt{\sigma_2^4 + 6I\sigma_2^2}}{18},\ q_1 = 0, \tag{28}$$

$$\text{(III)}\ \ p_1 = p_1^- = \frac{3I + \sigma_2^2 - \sqrt{\sigma_2^4 + 6I\sigma_2^2}}{18},\ q_1 = \pi. \tag{29}$$

(b) $I < \sigma_2^2/2$.

- When $\sigma_2 > 0$, the equilibrium points are

$$\text{(I)}\ p_1 = p_1^- = \frac{3I + \sigma_2^2 - \sqrt{\sigma_2^4 + 6I\sigma_2^2}}{18},\ q_1 = 0, \tag{30}$$

$$\text{(II)}\ p_1 = p_1^+ = \frac{3I + \sigma_2^2 + \sqrt{\sigma_2^4 + 6I\sigma_2^2}}{18},\ q_1 = \pi; \tag{31}$$

- when $\sigma_2 < 0$, the equilibrium points are

$$\text{(I)}\ p_1 = p_1^+ = \frac{3I + \sigma_2^2 + \sqrt{\sigma_2^4 + 6I\sigma_2^2}}{18},\ q_1 = 0, \tag{32}$$

$$\text{(II)}\ p_1 = p_1^- = \frac{3I + \sigma_2^2 - \sqrt{\sigma_2^4 + 6I\sigma_2^2}}{18},\ q_1 = \pi. \tag{33}$$

The stability of these equilibrium points is determined by the eigenvalues of the Jacobian matrix of the (p_1, q_1) equations in (22). It is easily deduced by performing the stability analysis that the equilibrium points corresponding to equations (24) and (27) are two saddle points, and others are center points. The heteroclinic orbits through the saddle point $(I/2, q_1^*)$ satisfies

$$H(p_1, q_1) = H\left(\frac{I}{2}, q_1^*\right). \tag{34}$$

We thus obtain the equations for heteroclinic orbits as follows

$$\text{Orbit A:}\ p_1 = \frac{\sigma_2^2}{4\cos^2 q_1}, \tag{35}$$

$$\text{Orbit B:}\ p_1 = \tfrac{1}{2}I. \tag{36}$$

The Melnikov function corresponding to equations (21) (ignoring the damping terms) can be found in reference [9] as system I

$$M = \int_{-\infty}^{+\infty} \Big\{ p_1^{1/2}(I - 2p_1)\sin q_1(t)[-2f\cos(2q_2(t))] - p_1^{1/2}\cos q_1(t) 2f(I - 2p_1) \times \sin(2q_2(t)) \Big\}\, \mathrm{d}t + p_1^{1/2}\cos q_1(t)_{((1/2)I,\, q_1^*)} \int_{-\infty}^{+\infty} 2f(I - 2p_1)\sin(2q_2(t))\, \mathrm{d}t. \tag{37}$$

The Melnikov function of orbit A: Substituting equation (35) into the second equation of equation (22), one can obtain $q_1(t)$ with initial condition $q_1(0) = \pi$ and $q_1(0) = 0$ depending on the sign of quantity σ_2.

If $\sigma_2 > 0$:

$$q_1(t) = \tan^{-1} \frac{\sqrt{2I - \sigma_2^2}}{\sigma_2} \tanh \frac{\sqrt{2I - \sigma_2^2}}{2} t. \tag{38}$$

If $\sigma_2 < 0$:

$$q_1(t) = \tan^{-1} \frac{\sqrt{2I - \sigma_2^2}}{\sigma_2} \tanh \frac{\sqrt{2I - \sigma_2^2}}{2} t + \pi. \tag{39}$$

One can thus plot the qualitative phase flow in different regions in the (I, σ_2) space, which is shown in Figure 2. The qualitative property of the system does not change under any small perturbation if the parameters lie in the region in (I, σ_2) space. There only exist center points in region 3, and so chaos does not occur in this region. We intend to use Melnikov's technique to analyze the behavior of two heteroclinic orbits A and B under perturbation. In order to calculate the Melnikov function, we need to have explicit expressions for the heteroclinic orbits. Expressions for $p_1(t)$ and $q_2(t)$ can be obtained from $q_1(t)$ as

$$p_1(t) = \frac{\sigma_2^2}{4} + \frac{2I - \sigma_2^2}{4} \tanh^2 \left(\frac{\sqrt{2I - \sigma_2^2}}{2} t \right), \tag{40}$$

$$q_2(t) = \tfrac{1}{2}(\sigma_2 - \sigma_1)t + q_{20}. \tag{41}$$

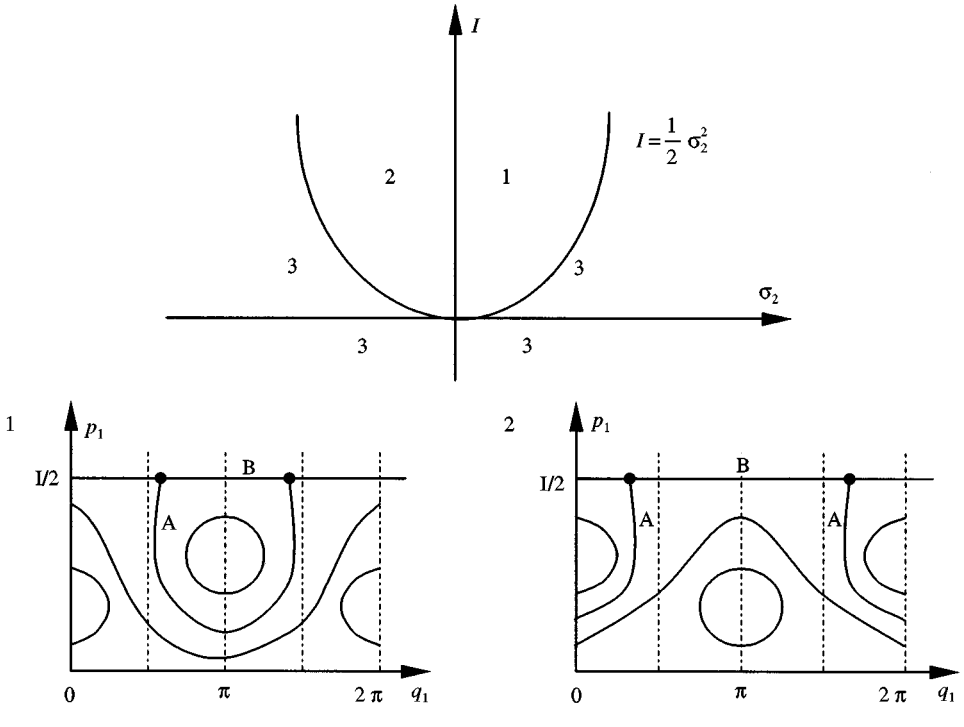

Figure 2. Parameter regimes in (I, σ_2) plane and partial associated phase portraits.

By using the above equations and letting $q_2(t) = \beta t + q_{20}$, the Melnikov integral corresponding to orbit A can be derived as

$$M_A = 2f \int_{-\infty}^{+\infty} (I - 2p_1) p_1^{1/2} \sin[q_1(t) + 2q_2(t)]\, \mathrm{d}t - \sigma_2 f \times \int_{-\infty}^{+\infty} (I - 2p_1) \sin[2q_2(t)]\, \mathrm{d}t. \tag{42}$$

By using the nature of the even and odd function and the expression in equations (38)–(41), the Melnikov function can be calculated as

$$M_A^{\pm} = -8\pi f \beta^2 \sin(2q_0) \operatorname{cosech}\left(\frac{2\pi\beta}{\sqrt{2I - \sigma_2^2}}\right). \tag{43}$$

Substituting $\beta = \frac{1}{2}(\sigma_2 - \sigma_1)$ into equation (43), one can obtain

$$M_A^{\pm} = -2\pi f (\sigma_2 - \sigma_1)^2 \sin(2q_0) \operatorname{cosech}\left(\frac{\pi(\sigma_2 - \sigma_1)}{\sqrt{2I - \sigma_2^2}}\right). \tag{44}$$

It is easy to see that the Melnikov function has a simple zero with respect to q_{20} provided the coefficient of $\sin(2q_{20})$ is not zero, that is $\sigma_2 \neq \sigma_1$ and $I > \frac{1}{2}\sigma_2^2$. In this case, the heteroclinic orbit A breaks with transversal intersections under perturbation, which leads to a Smale horseshoe type of chaos. The second condition indicates that the energy in the system needs to exceed a certain minimum value before chaotic motions can occur.

The Melnikov function of orbit B: Substituting the equation of orbit B, that is $p_1 = \frac{1}{2}I$ into equation (37), we can simply derive:

$$M_B^{\pm} \equiv 0. \tag{45}$$

Thus, one concludes that orbit B does not break under small perturbation.

3. EXPERIMENT

3.1. THE TEST RIG AND MEASURING PROCEDURE

The test rig consists of four components, which are T-shaped beam–mass structure, excitation system, data acquisition system and signal processing system. The schematic of the experimental set-up is shown in Figure 3. The mechanical structure is excited by a PR9270 vibration exciter driven by a power amplifier. The excitation signals are generated by a sinusoidal signal wave synthesizer. The excitation amplitude is held constant (as the excitation frequency is swept) by the computer-controlled feedback loop. Two accelerometers, with each mounted on one beam respectively, are used to pick up the vibratory signals of the transverse displacements of the structure. The signals are monitored on a digital oscilloscope, recorded by a cassette recorder, and sent to an IBM PC which acquired data through a 16-bit analog-to-digital converter. A sampling frequency of 376 Hz is used and 2048 points per team are collected. The acquired data stored in the IBM PC are directly analyzed by a FFT algorithm.

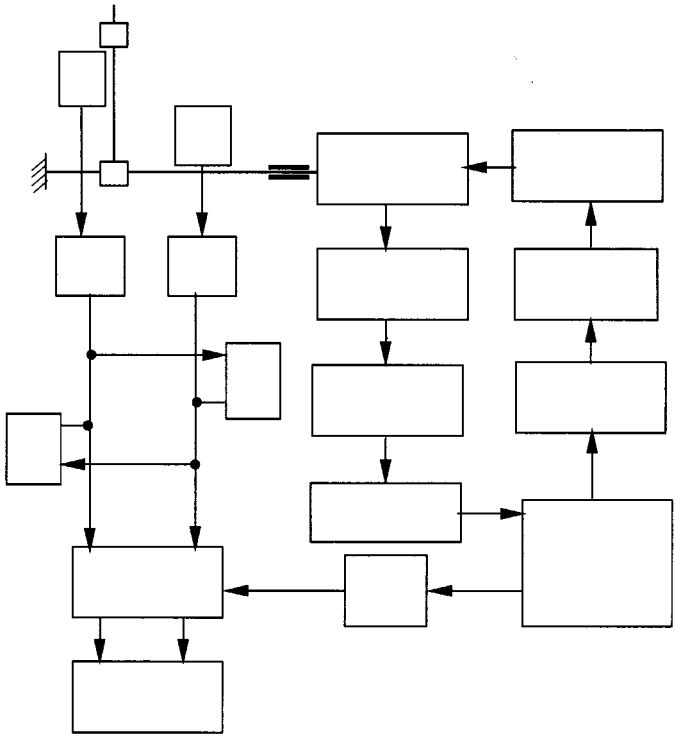

Figure 3. A sketch of the experimental set-up. Note: accelerometers—1, B & K2635 charge amplifier—2, digital oscilloscope—3, casette recorder—4, Poincare map pulse generator—5.

The linear resonant frequencies of the structure were determined by using a random excitation. When $L_1 = 350{\cdot}7$ mm and $H_1 = 190{\cdot}3$ mm, they were $f_1 = 12{\cdot}69$ Hz and $f_2 = 6{\cdot}25$ Hz. The modal damping coefficients were found to be very small by performing parameter-identification studies, and so the linear resonant frequencies should be very close to the linear natural frequencies.

3.2. THE REGIMES OF APPEARANCE OF CHAOTICALLY MODULATED MOTIONS

Figure 4 shows the experimentally obtained variation of the excitation amplitude with the excitation frequency on which the structure appeared chaotically amplitude-modulated motions. The linear resonant frequencies of the structure were $f_1 = 12{\cdot}69$ Hz and $f_2 = 6{\cdot}25$ Hz. As is well known, the chaotic motions are very sensitive to initial conditions. The procedure for determining the curves in Figure 4 was as follows. We first choose an excitation frequency and kept it constant, then slowly increased excitation amplitude in small increments. At each step the excitation output by the vibration exciter was held constant by the computer-controlled feedback loop. We waited and observed the stationary response of the structure by on-line signal analyses after the transient response fully died out. Once chaotically amplitude-modulated motion appeared, the excitation amplitude was noted. This threshold value is of major concern in performing theoretical analyses and numerical simulations. Then we reduced the excitation

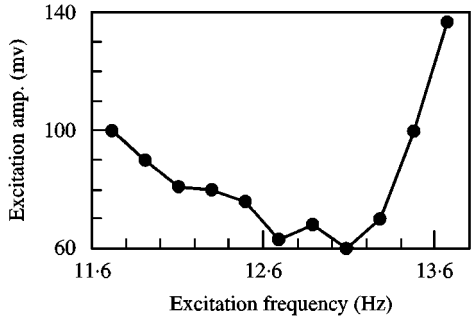

Figure 4. Variation of the excitation amplitude with the excitation frequency for appearance of chaotically amplitude-modulated motions.

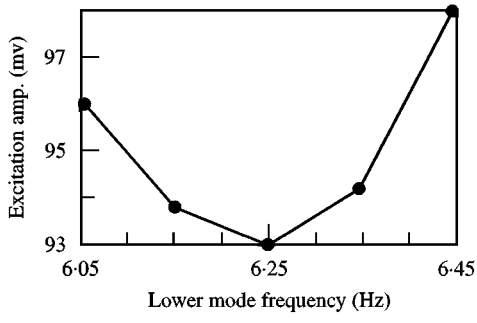

Figure 5. Variation of the excitation amplitude with the lower mode frequency for appearance of chaotically amplitude-modulated motions.

amplitude to zero. After the response was fully trivial, we swept the excitation frequency in small increments to another value, then repeated the above procedure such that we obtained the critical value in this excitation frequency. Care was taken to ensure that the small increments were properly placed so that a critical value was not exceeded. Figure 5 shows the experimentally obtained variation of the excitation amplitude with the lower natural frequency for appearance of chaotically amplitude-modulated motions. The higher resonant frequency of the structure and the excitation frequency were $f_1 = 12{\cdot}50$ Hz and $f = 12{\cdot}51$ Hz. According to definition (5), this figure shows the excitation amplitude against the internal mistunings (or detunings) σ_2. In some sense, it indicates the total energy in the system against the internal mistunings. Compared with Figure 2 obtained by theoretical analysis, it shows good qualitative agreement with the theoretical predictions.

3.3. PARAMETRIC RESONANCE RESPONSE

In the region of parametric resonance to the lower mode, the periodic motions, periodically amplitude-modulated motions and chaotically amplitude-modulated motions were observed as one of the control parameters in the system varied. In conducting tests, it was easy to vary either the excitation amplitude or the

excitation frequency. The reason for this procedure was to see the routes to chaos through parameter changes. The characteristic precursor to chaotically amplitude-modulated motions was found to be the appearance of periodically amplitude-modulated motions. Figure 6 shows the time histories of two modes as the excitation amplitude increased from zero, while the Fourier spectra of the corresponding response are shown in Figure 7. As the excitation amplitude was increased from zero, the response remained trivial until a critical value was exceeded. Increasing the excitation amplitude beyond this value caused periodic response (see Figure 6(a)). Beyond a certain level of the excitation amplitude, the periodic motions ceased to exist. We saw periodically amplitude-modulated

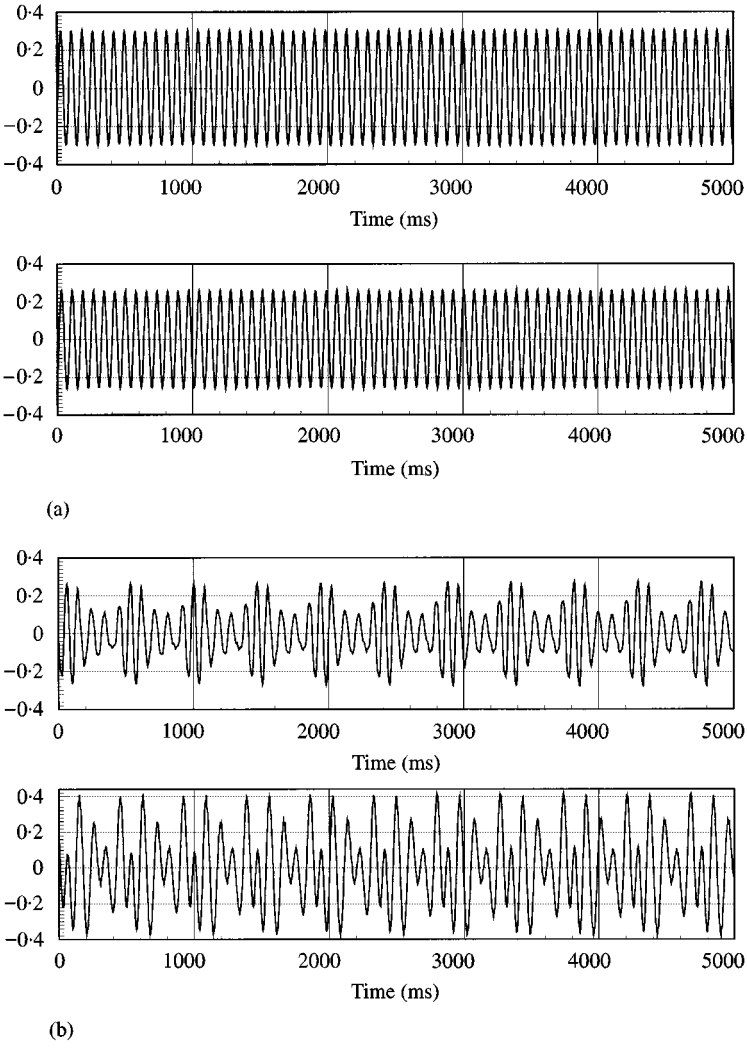

Figure 6. Time histories of the higher mode $f_1 = 12{\cdot}69$ Hz and the lower mode $f_2 = 6{\cdot}25$ Hz for excitation frequency $f = 12{\cdot}6953$ Hz as excitation amplitude increases. Excitation amplitude (a) 55 mV, (b) 63·5 mV, (c) 70 mV, (d) 77·5 mV, (e) 83 mV.

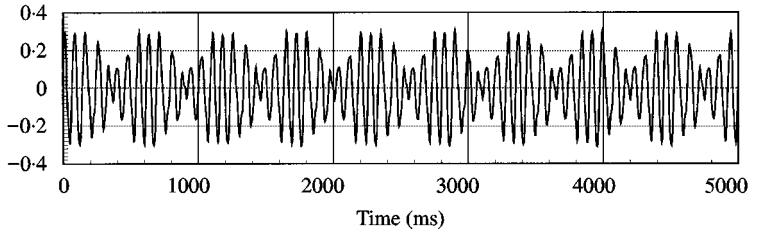

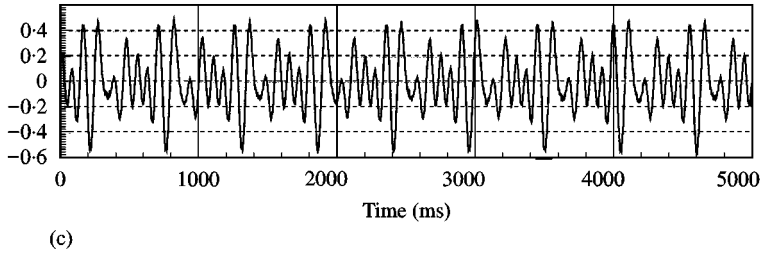

(c)

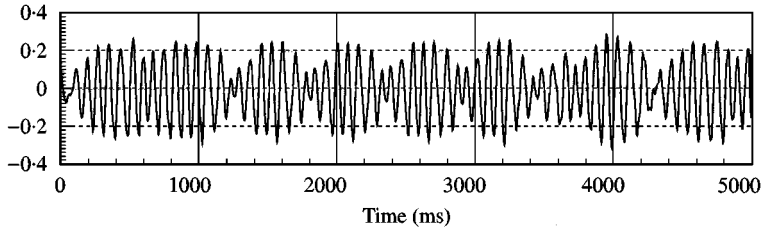

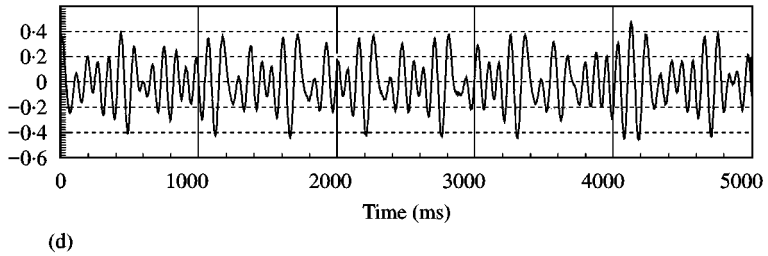

(d)

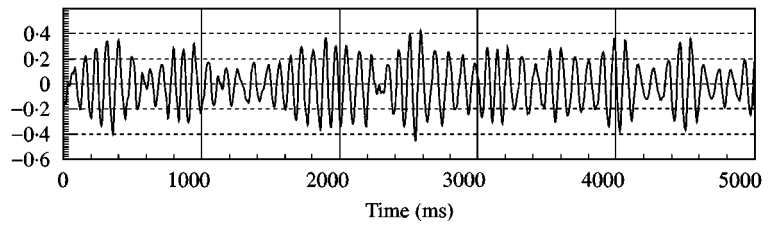

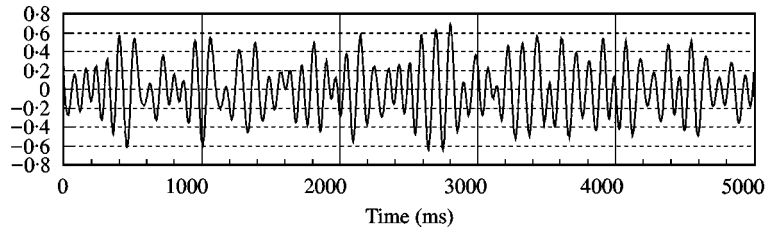

(e)

Figure 6. Continued.

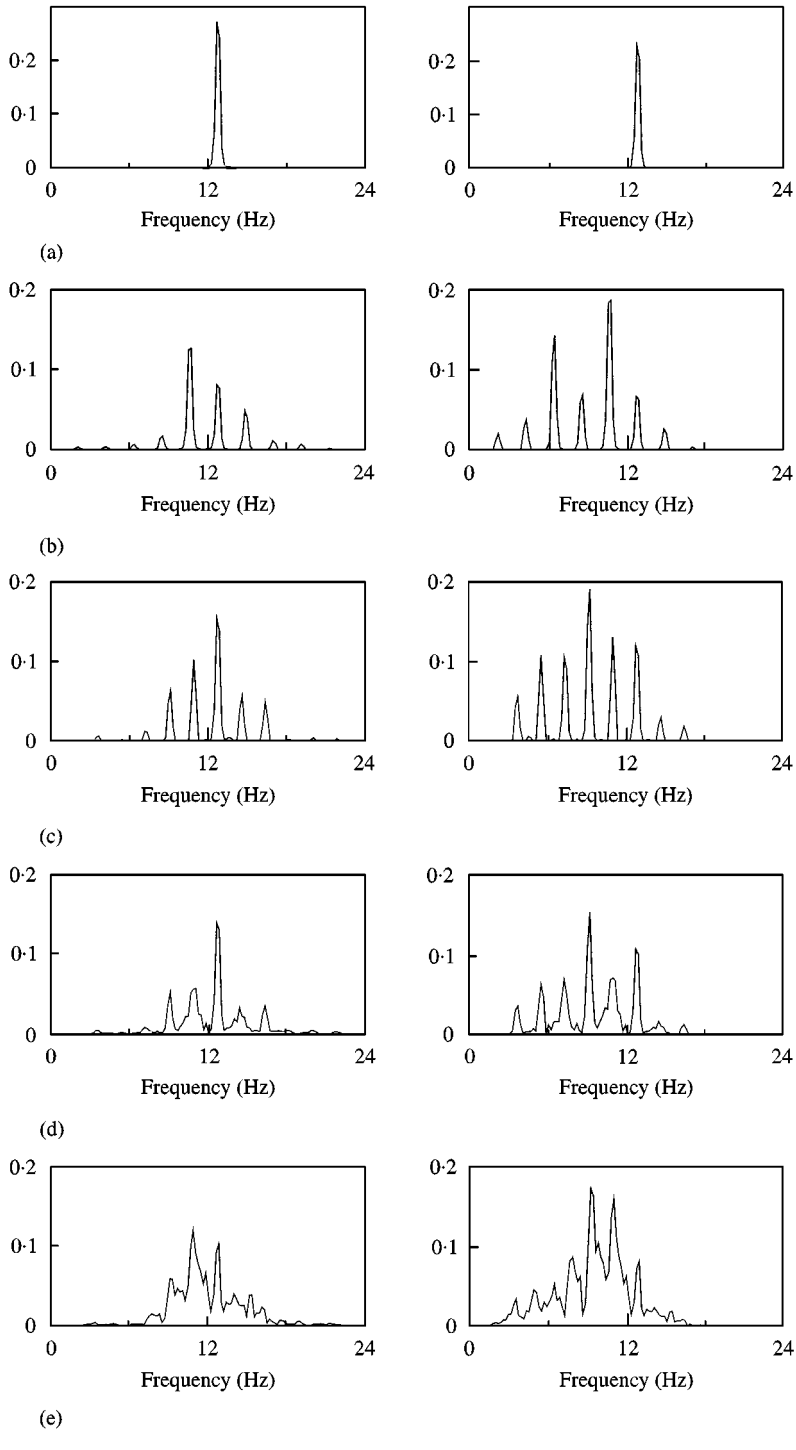

Figure 7. The Fourier spectra of the corresponding responses shown in Figure 6. Excitation amplitude (a) 55 mV, (b) 63·5 mV, (c) 70 mV, (d) 77·5 mV, (e) 83 mV.

motions beyond the excitation amplitude (see Figure 6(b)). The response spectrum in Figure 7(b) shows discrete spectral lines at $f \pm n\delta f$ and $1/2f \pm n\delta f$, where $n = 0, 1, 2, 3, \ldots$ δf is related to the modulation frequency in the corresponding averaged system, while Enrich [10] called it spontaneous sidebands in analyzing the rub motions in rotor dynamics. As excitation amplitude increased further, it was found that there existed a range of excitation amplitudes for periodically amplitude-modulated motions. Figure 6(c) shows the non-linear response when the amplitude of excitation signals was 70 mV. From the corresponding frequency spectra shown in Figures 7(b) and (c), it was easy to see that their modulation frequencies were different. One can thus conclude that the modulation frequencies are different as the control parameter varies. As the excitation amplitude increased further beyond another critical value, the periodically amplitude-modulated motions disappeared. We observed chaotically amplitude-modulated motions (see Figure 6(d)). The spectrum in Figure 7(d) shows a broadband character around the excitation frequency, indicating that the motion was chaotic at this frequency. As excitation amplitude increased to 83 mV, the response of structure is shown in Figure 6(e). It is obviously chaotically amplitude-modulated motions. In Figure 8, a representative Poincare map is shown for $f_1 = 12{\cdot}5$ Hz, $f_2 = 6{\cdot}05$ Hz, $f = 12{\cdot}69$ Hz and excitation amplitude is 97 mV. The Poincare map is plotted on the amplitude of the higher mode and that of the lower mode plane.

During experiments, we occasionally observed the alternate appearance of periodically modulated motions and chaotically modulated motions. When the system parameters and excitation parameters were fixed as constant, we noted that the periodically modulated motions and chaotically modulated motions appeared alternately. We ran for a long time after we thought the response of structure was stationary. This scenery was repeated in a range of excitation amplitudes. The results are shown in Figure 9.

3.4. DEPENDENCE ON INITIAL CONDITIONS

For a system with multiple steady-state solutions, the possible solution is determined by the initial condition. In fact, many dynamic problems are sensitive to initial conditions. During the experiment, we gradually increased the excitation amplitude, and let the system settle to steady responses at a certain value, then

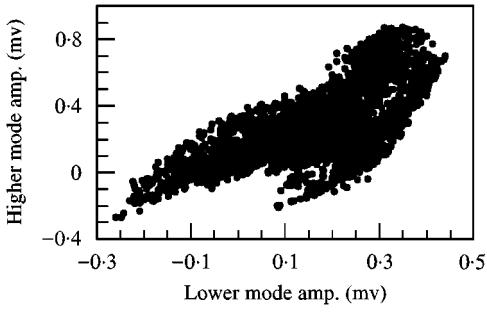

Figure 8. Poincare map on the u_1–u_2 plane.

suddenly decreased the excitation amplitude to another value, and kept it unvaried. We observed the system settling to a qualitatively different behavior. The motions may change into periodically or chaotically amplitude-modulated motions, while the previous motions at the same excitation amplitude were periodic. In some cases, the response changed into chaotically amplitude-modulated motions, whereas the previous motions at the same excitation amplitude were periodically amplitude-modulated motions. These observations indicated that the system settled to a different attractor depending on the starting conditions. For

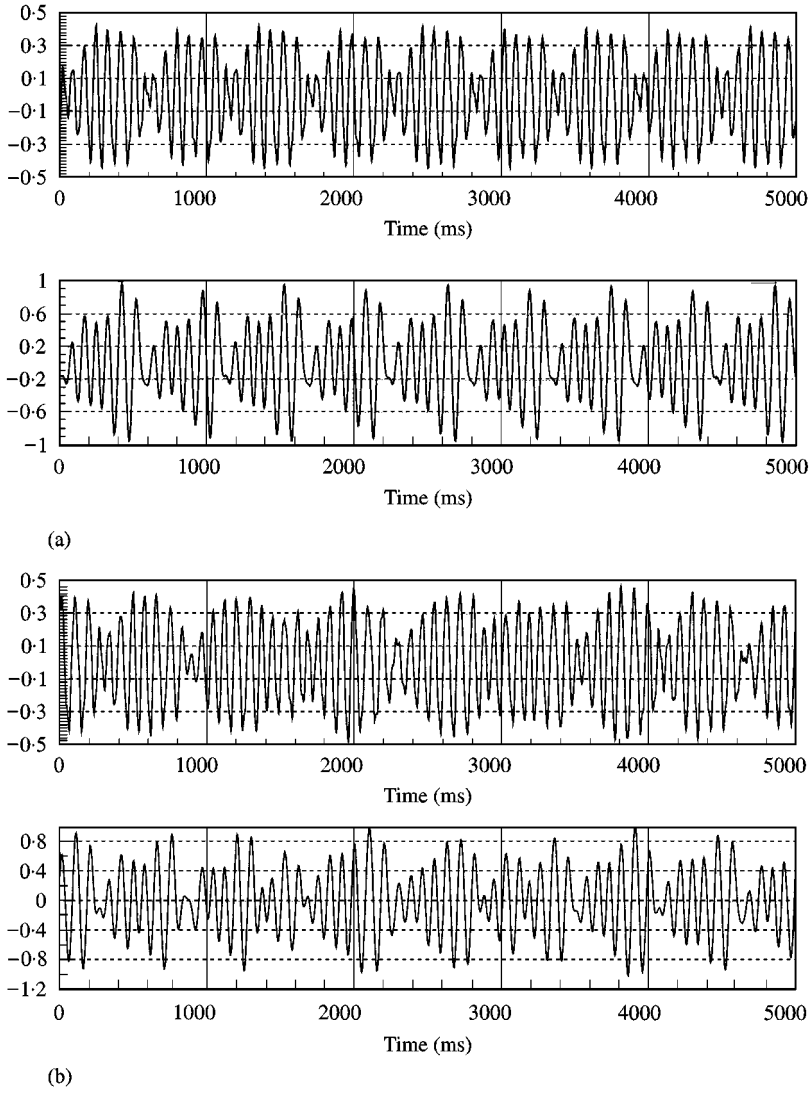

Figure 9. The alternation of periodically and chaotically amplitude-modulated motions for the resonant frequency of higher mode $f_1 = 12{\cdot}5$ Hz, the resonant frequency of the lower mode $f_2 = 6{\cdot}05$ Hz and excitation frequency $f = 12{\cdot}69$ Hz at the fixed excitation amplitude. Excitation amplitude (a) 77·3 mV, (b) 77·3 mV.

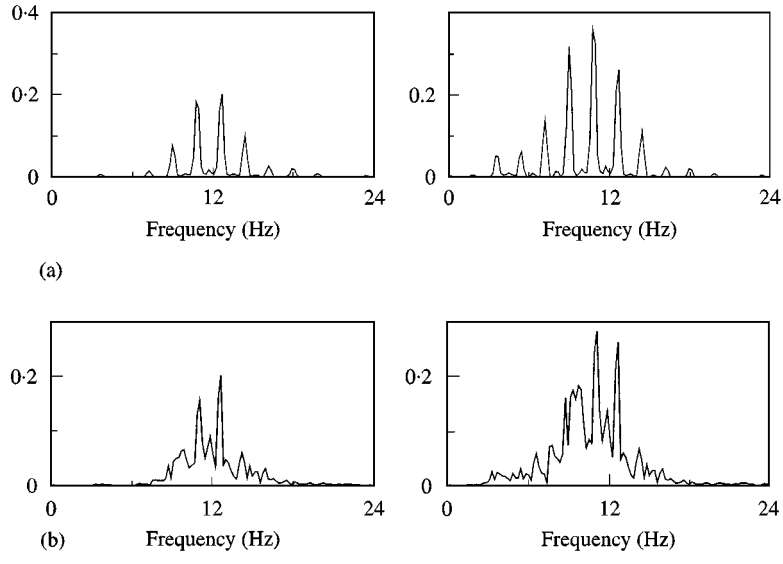

Figure 9. Continued.

a non-linear mechanical system, multiple attractors are common, and indeed there may be periodic and chaotic attractors coexisting, for example. The appropriate operation condition is of crucial importance, because the motion is very sensitive to initial conditions.

4. CONCLUSIONS

The local and global bifurcation of a two-d.o.f. non-linear system with quadratic non-linearities is theoretically investigated, in case of a one-to-two internal resonance and a principal parametric excitation of the lower mode. The method of multiple scales is used to derive four first-order autonomous ordinary differential equations for the modulation of the amplitudes and phases. The steady state solutions of the modulated equations and their stability are investigated. The trivial solutions lose their stability through pitchfork bifurcation giving rise to non-trivial solutions. The Melnikov's method is employed to detect the parameter values at which the averaged system exhibits complicated dynamics. Finally, in order to observe amplitude-modulated motions of the structure, experiments are conducted. The experimental observations may offer better understanding of the amplitude-modulated motions to the physical phenomenon. The experimental results are in good qualitative agreement with theoretical predictions.

ACKNOWLEDGMENT

This research was supported by the National Natural Science Foundation of China.

REFERENCES

1. A. H. Nayfeh 1987 *Journal of Sound and Vibration* **119**, 95–109. Parametric excitation of two internally resonant oscillators.
2. A. H. Nayfeh and J. F. Nayfeh 1990 *Physics of Fluids* **A2**, 1635–1648. Surface waves in closed basins under principal and autoparametric resonances.
3. Z. C. Feng and P. R. Sethna 1990 *Dynamics and Stability of Systems* **5**, 210–225. Global bifurcation and chaos in parametrically forced systems with one–one resonance.
4. Z. C. Feng and S. Wiggins 1993 *Z Angew Math Phys* **44**, 201–248. On the existence of chaos in a class of two degree-of-freedom, damped, strongly parametrically forced mechanical systems with broken O(2) symmetry.
5. B. Banerjee and A. K. Bajaj 1997 *Acta Mechanica* **124**, 131–154. Amplitude modulated chaos in two degree-of-freedom systems with quadratic nonlinearities.
6. B. Balachandran and A. H. Nayfeh 1991 *Nonlinear Dynamics* **2**, 77–117. Observations of modal interactions in resonantly forced beam–mass structure.
7. J.-C. Ji 1997 *Ph.D. Thesis, Tianjin University*. Bifurcation and chaos in a parametrically excited two degree-of-freedom nonlinear oscillating system: theoretical analyses and experimental investigations (in Chinese).
8. A. H. Nayfeh 1973 *Perturbation Methods*. New York: Wiley-Interscience.
9. S. Wiggins 1990 *Global Bifurcations and Chaos—Analytical Methods*. New York: Springer-Verlag.
10. F. F. Enrich 1992 *ASME Journal of Vibration and Acoustics* **114**, 498–505. Spontaneous sidebanding in high speed rotor dynamics.